FIRE DETECTION IN BORNEO USING HIMAWARI/AHI

Shun Sato [1] and Masayuki Matsuoka [*2]
[1] Graduate Student, Department of Information Engineering, Mie-University, Mie, Japan
1577 Kurimamachiya, Tsu, Mie 514-8507 Japan
Email: 422M517@m.mie-u.ac.jp

[*2] Associate Professor, Department of Information Engineering, Mie-University, Mie, Japan
1577 Kurimamachiya, Tsu, Mie 514-8507 Japan
Email: matsuoka@info.mie-u.ac.jp

KEY WORDS: forest fire, Himawari/AHI, threshold-based algorithm

ABSTRACT: Forest fires cause global warming and air pollution, hence, early detection is required. We developed a fire detection algorithm using Advanced Himawari Imager (AHI) onboard Himawari. This algorithm was applied for several AHI scenes observed in 2018. In comparison with the fire product by Moderate Resolution Imaging Spectroradiometer (MODIS), this algorithm showed higher detection accuracy both in the area and location of the fire. Time series of brightness temperature indicated the lower detectability in night-time, probably due to the temperature decrease in fire areas. Histograms were created from multiple time series data, and the thresholds for clouds and fires were redefined based on these histograms to improve the accuracy.

1. INTRODUCTION

1.1 Motivation

In Southeast Asia, forest fires have occurred frequently by slash-and-burn agriculture and plantation development. Forest fires emit toxic nitrogen dioxide, sulfur dioxide, and large amounts of carbon dioxide, causing problems such as air pollution and global warming. Early detection of fires is therefore important.

1.2 Aims

In this study, fire detection was conducted using the AHI sensor onboard the Himawari satellite. This algorithm was modified based on the fire detection algorithm of Advanced Baseline Imager (ABI) onboard Geostationary Operational Environmental Satellites-R (GOES-R) series of satellite. Fire detection has also been performed by MODIS onboard Terra and Aqua, but it can observe fires only twice a day. The AHI has a high temporal resolution suitable for early fire detection. The AHI also has many observations of spectral bands, so it is expected to be able to detect fires with higher accuracy.

1.3 Related Work

Mizutani et al. (2017) conducted a fire detection study on fire in the Kingdom of Buryat by analyzing the spectrum of the AHI at thermal infrared wavelengths. They created a function to extract the radiative energy from bands 7 and 13, and the fire was detected based on the energy. As a result, they were able to detect fires at a minimum area of 0.2 km^2.

Xu et al. (2017) developed the processing system to identify active fires from the AHI data and retrieved the fire radiative power (FRP) based on the Fire Thermal Anomaly (FTA) algorithm and FRP retrieval method developed using the Spinning Enhanced Visible and Infrared Imager (SEVIRI).

2. DATA

In this study, Borneo was extracted from the full disk image of Himawari-8 every 10 minutes for the year 2018 (Bessho et al., 2017). We used band 3 (the central wavelength range is 0.64 μm) in the visible wavelength, and bands 7 (3.9 μm), 14 (11.2 μm), and 15 (12.3 μm) in the infrared wavelength range. Bands 3, 7, and 14 were used for fire detection, and band 15 for cloud detection. The extracted area was from 108°E to 120°E in longitude, and from 5°S to 8°N in latitude, which includes Borneo Island (Figure 1).

Table 1. Spectral bands of Himawari/AHI and their applications

Band	Wavelength	Application
3	0.63914 μm	Fire and Cloud
7	3.8853 μm	Fire and Cloud
14	11.2395 μm	Fire and Cloud
15	12.3806 μm	Cloud

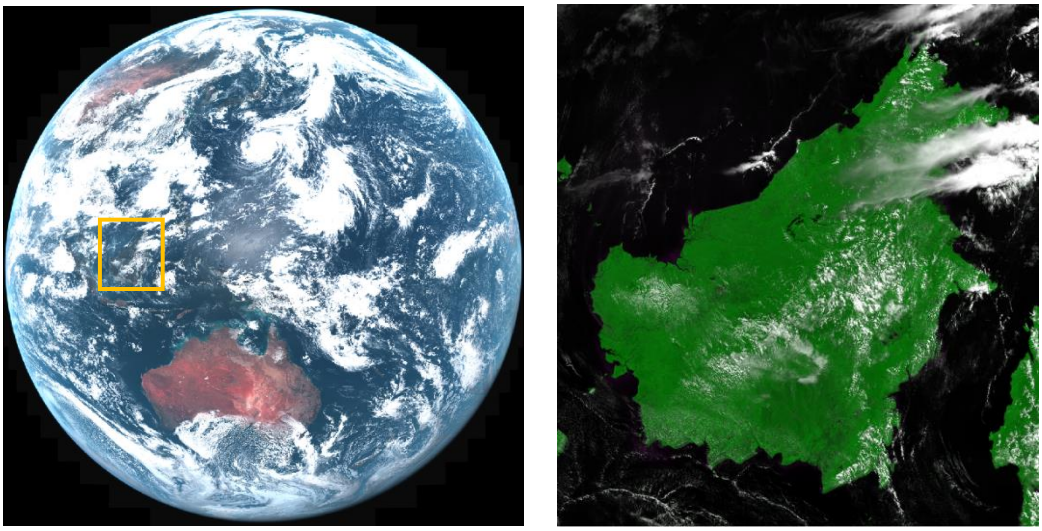

Figure 1. True colour image of the AHI, the site of this study

In addition, the MODIS land cover classification map, MCD12Q1, was used to remove water pixels. MODIS fire products, MOD14A1 and MYD14A1, were used to evaluate the accuracy of the detected fires (NASA, 2023).

3. METHOD

3.1 Fire Detection

The GOES-R/ABI has similar specifications to the AHI. Therefore, in this study, fire detection was performed based on the GOES-R fire detection algorithm by Schmidt et al. (2012). This algorithm detects fires by comparing fire pixels with surrounding non-fire pixels (hereafter referred to as background pixels) using the radiance of bands 7 and 14. According to Planck's radiation law, the higher the temperature, the shorter wavelength the peak of the radiance shifts to and the larger the radiance is. This means that fire can be detected by looking at the difference in radiance between bands 7 and 14. Comparing this difference with background pixels, fire can be detected because fire has different brightness temperature and spectral radiance from background non-fire area. Pixels with large sunlight reflections, pixels with missing values, water areas, and clouds were removed to reduce the false detection of fire. In addition, by using a dynamic threshold that takes the time variation of the temperature into account, robustness to differences in location, season, and time can be expected. The outline of the algorithm is explained in the following subsections.

Removal of Non-target Pixels: We removed the areas of large sunlight reflections, missing values, water, and clouds because these areas will cause false detection of fires. Sunlight reflections were removed from the solar zenith angle, and water areas were removed as non-target pixels using the MCD12Q1 land cover classification dataset. Clouds were also removed from the AHI data through a series of threshold tests using brightness temperatures of bands 7, 14, and 15, and only during the daytime, reflectance of band 3.

Calculation of Statistics of Background Pixels: Statistics of brightness temperature and radiance were calculated for background pixels. The area of background pixels was expanded in a square shape until at least 20 per cent of the pixels in the rectangular area were valid pixels (other than water and clouds). if there were not enough valid pixels after 20 expansions, the fire determination of the target pixel was not performed as an algorithm failure. If the background pixels

were determined successfully, statistics such as the mean and standard deviation of brightness temperature and reflectance were calculated. Using these statistics, a threshold value was set, and fire detection was performed.

Fire Area and Temperature Estimation: Dozier's method (1981) estimates the temperature and area of fire simultaneously by simulating the radiance by shifting the temperature and the area of the fire and comparing it with observed radiance. This allows us to calculate the scale of the fire within a single pixel (approximately 1 km^2).

Elimination of False Fire Pixels: To eliminate pixels where clouds were falsely detected as fire, the albedo and brightness temperature of the target pixel were compared to the statistics of the background pixels, respectively, to determine the cloud pixel and sunglint pixel. The determined pixels were treated as low-confidence fire pixels as described below.

Determination of Fire Confidence Level: The algorithm gives a confidence level (low, medium, and high) of detection to each fire pixel. The difference in brightness temperature between the fire and the background increases in proportion to the size of the fire. Therefore, the reliability of the fire was evaluated by comparing it with the statistics of the background pixels.

3.2 Improvement of Fire Detection Accuracy

In comparison with MODIS fire detection products, we found several issues in our algorithm, such as the false detection of non-fire locations as fires and the inability to detect fires at night. Therefore, in this study, we worked on further fire detection by setting thresholds depending on the time of day.

Time-varying Threshold for Cloud Detection: In the current detection method, clouds were often inaccurately detected as fire, especially at night. Therefore, the first improvement was to create a threshold that would change over time for cloud removal. First, we created histograms of brightness temperature and reflectance over land at each time of the day using monthly data. From these histograms, the time series of each 10 percentile of the histogram was extracted. Thresholds were determined based on the percentile closest to the original thresholds used in cloud detection tests. Since the decided time-varying threshold was not smooth, the moving average was applied using a window size of ±1 hour. For each of the moving average thresholds, adjustments were made to the thresholds for improving the cloud detection accuracy. Time-varying thresholds were applied to the brightness temperature of bands 7, 14, and 15, and the difference of brightness temperature between bands 7 and 14. This new method was applied at night from 6 p.m. to 7 a.m. local time. For daytime data, the fixed threshold was determined by visual investigation.

Time-varying Threshold for Fire Detection: Time-varying threshold was also determined for the fire detection using cloud-free pixels, based on a similar method to the cloud detection described above. This was done for bands 7 and 14, and the difference between bands 7 and 14, which were primarily used for fire detection.

Re-detection of Fires with Time-varying Thresholds: Fire detection was based on the new time-varying thresholds created in the previous subsection. The unique threshold was applied by time to all valid pixels, excluding invalid pixels.

4. RESULTS AND DISCUSSION

4.1 Fire Detection by Fixed Thresholds

Figure 2 is the area detected as fire in southern Borneo at 11:00 local time on August 18, 2018. Figure 2(a) shows the fire detection results using the fixed thresholds, Figure 2(b) shows the MODIS fire detection results on the same day, and Figure 2(c) is a high-resolution satellite image from Sentinel-2.

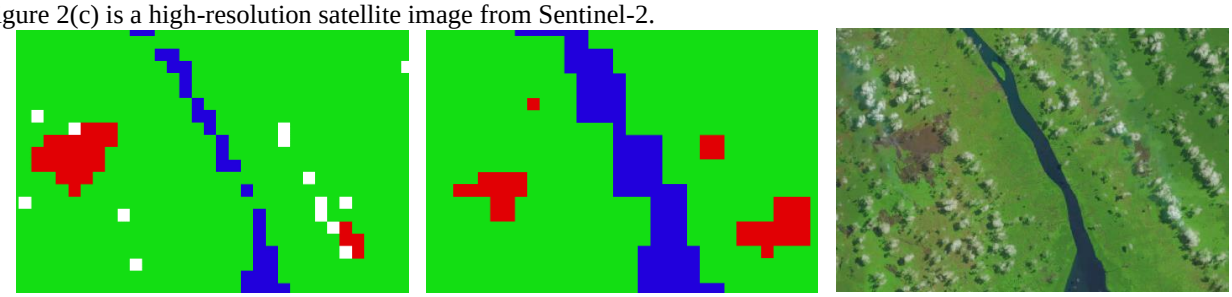

(a) AHI (b) MODIS (c) Sentinel-2

Figure2. Comparison of detection (8/18/2018 at 11:00 WITA)

In Figure 2(c), we can see the large fire located on the left side of the image. Both the AHI and MODIS can detect the fire, but the AHI fire was closer in location and similar in shape. This indicates that the AHI was superior to MODIS because of its higher observation frequency and higher accuracy.

However, fire detection at night was problematic. Figure 3 shows the temperature difference of bands 7 and 14 at 22:30 local time on August 18, 2018, overlaid with the fire detection result.

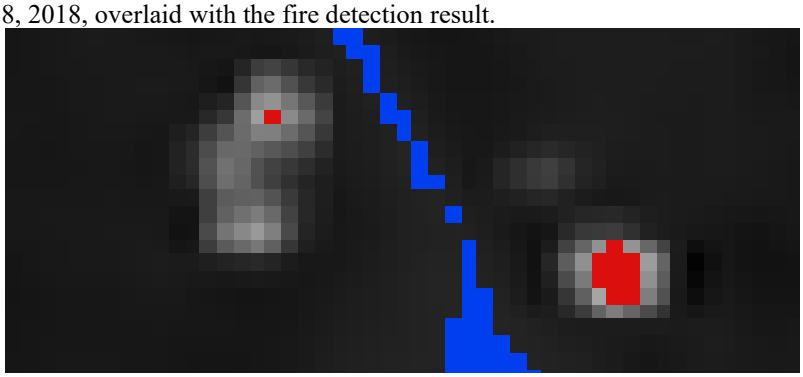

Figure 3. Difference of the brightness temperature in bands 7 and 14. Detected fire pixels were overlaid (8/18/2018 at 22:30 WITA).

The bright pixels indicate a large difference of brightness temperature between bands 7 and 14, most likely a fire. In Figure 3, although some pixels were detected as fire, we considered the fixed thresholds insufficient to detect the fire at night-time. Similar results were obtained for other times and locations. One possible reason is that the brightness temperature drops significantly at night. Figure 4 shows a graph of the brightness temperature for band 14.

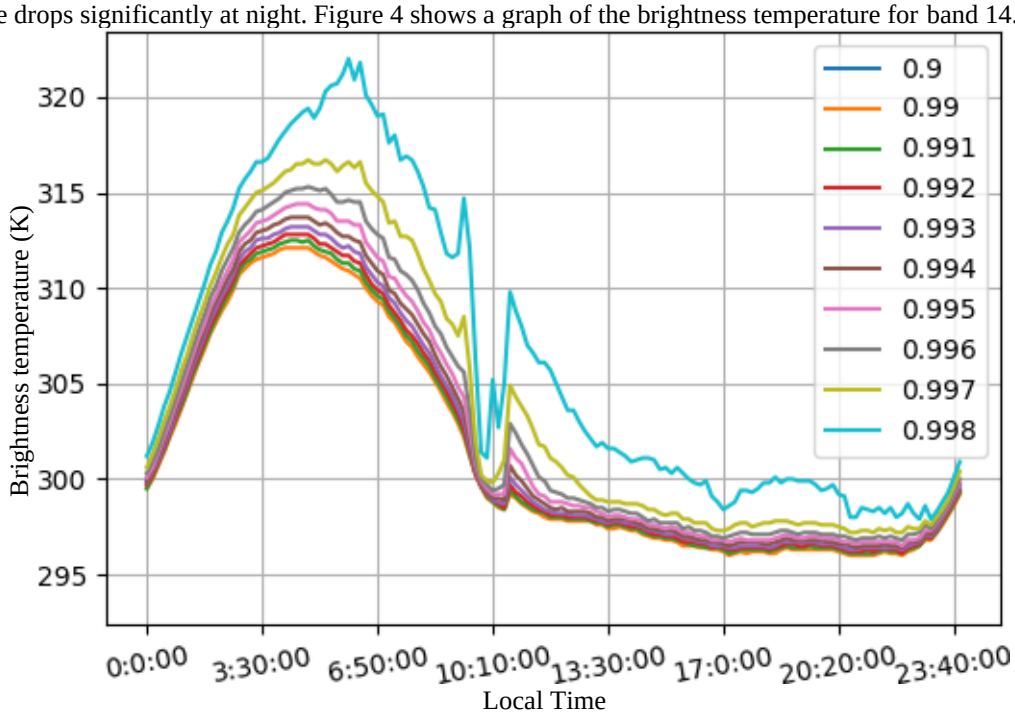

Figure 4. Graph of the brightness temperatures of band 14 on 08/18/2018.

Figure 4 shows that there is a large variation in brightness temperature by time of the day. In the case of fixed thresholds, it is difficult to detect fires at night when brightness temperatures decrease.

4.2 Fire Detection by Time-varying Thresholds

Time-varying Threshold for Cloud Detection: We adopted the 40 percentile as the time-varying threshold for band 7 and the difference between bands 7 and 14, and the 70 percentile for bands 14 and 15. Figure 5 compares the cloud detection results between fixed and time-varying thresholds at night. The background image is the difference in brightness temperature between bands 7 and 14 at the same time of day. In Figure 5(a), pixels with large temperature difference were not detected as the cloud in fixed thresholds, but it was detected in time-varying thresholds. Thus, it was useful to create a time-varying threshold for detecting clouds at night.

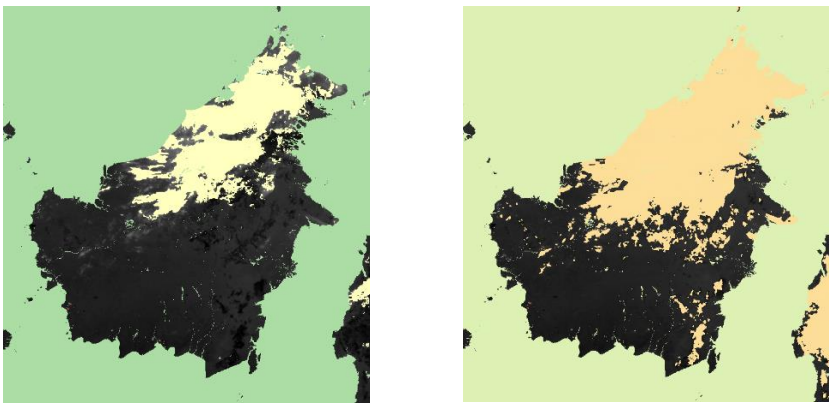

(a) Fixed threshold (b) Time-varying threshold

Figure 5. Comparison of cloud detection results by fixed and time-varying thresholds (8/18/2018 at 22:30 WITA)

Time-varying Threshold for Fire Detection: The threshold values were 99.5 percentile for bands 7 and 14 and 95 percentile for the difference between bands 7 and 14. Figure 6 compares the fire detections by fixed and time-varying thresholds. Figure 6(c) shows the central part of Figure 6(a) where undetected fires were located, shown in Figure 3. These fires can be detected clearly in Figure 6(b). This indicates that fire can be detected even at night by using a time-varying threshold for clouds and fire. This indicates that fire can be detected even at night by using a time-varying threshold for clouds and fire.

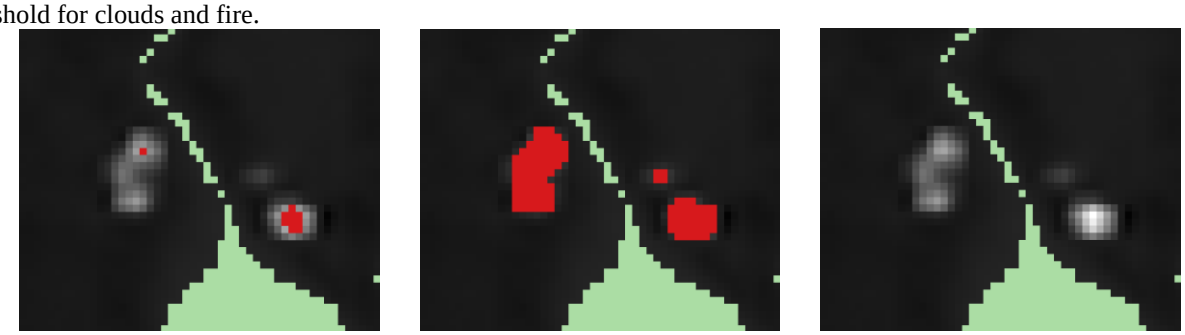

(a) Fixed thresholds (b) Time-varying thresholds (c) Difference between bands 7 and 14

Figure 6. Comparison of fire detection by fixed and time-varying thresholds (8/18/2018 at 22:30 WITA)

Re-detection of Fires with Time-varying Thresholds: Figure 7 shows the time series of fire detection in two-hour intervals using time-varying thresholds.

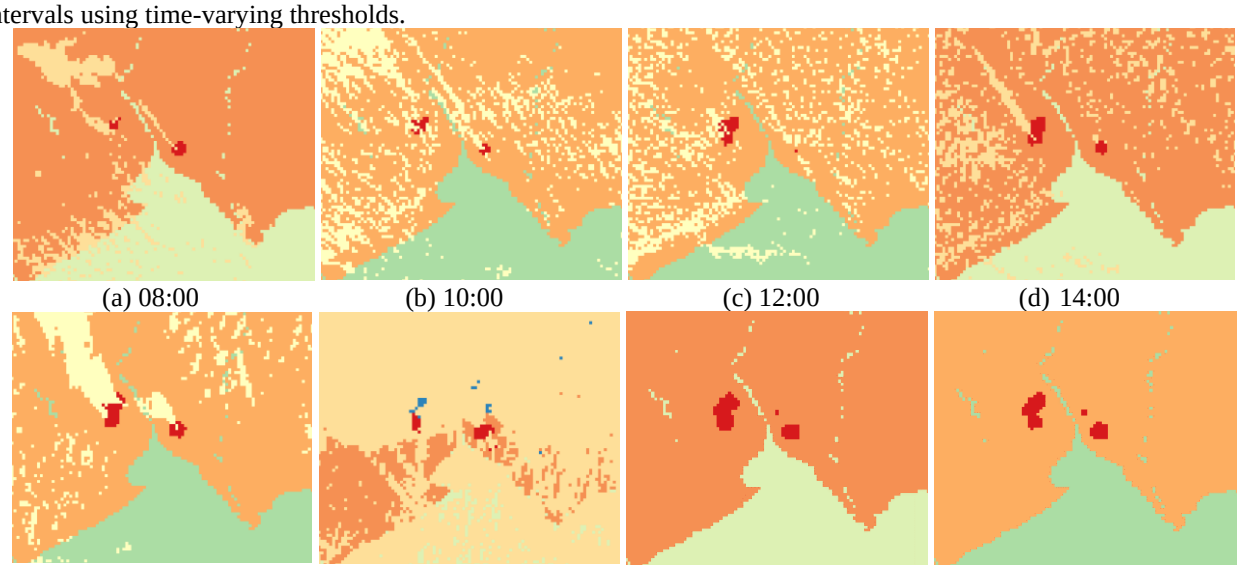

(a) 08:00 (b) 10:00 (c) 12:00 (d) 14:00

(e) 16:00 (f) 18:00 (g) 20:00 (h) 22:00

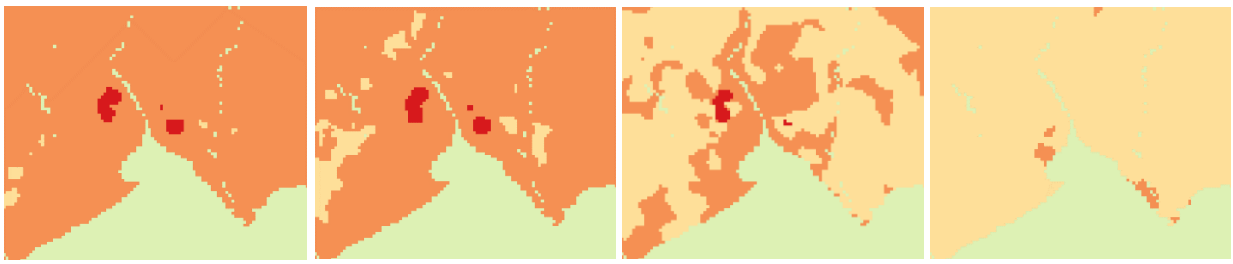

(i) 00:00 (j) 02:00 (k) 04:00 (l) 06:00

Figure 7. Time series of fire detection results for 22 hours in 2-hour intervals (8/18-19/2018). The red colour shows the fire.

It could be seen from Figure 7 that we have been able to detect almost the same locations for the fire location. However, most of the area has been unrealistically occupied by clouds at sunset in Figure 7(f) and sunrise in Figure 7(l). This may be because the solar zenith angle has a significant impact on the reflectance data at sunrise and sunset.

5. CONCLUSION

We developed the fire detection algorithm for Himawari/AHI. Compared to existing MODIS fire products, both observation frequency and accuracy were superior. In addition to the fixed thresholds algorithm detection, fire detection during night-time was made possible by setting time-varying thresholds for clouds and fire, respectively.

Further investigations include the detailed setting of temporal varying thresholds and the elimination of false positives by comparing sequential data thanks to the high temporal resolution of the AHI.

ACKNOWLEDGEMENTS

This research was funded by the JSPS KAKENHI under grant numbers JP20K20487 and JP22H05004. The Himawari-8 data used in this study was provided by the Japan Meteorological Agency through the NICT Science Cloud.

REFERENCES

Bessho, K., Date, K., Hayashi, M., Ikeda, A., Imai, T., Inoue H., Kumagai, Y., Miyazaki, T., Murata, H., Ohno, T., Okuyama, A., Oyama, R., Sasaki, Y., Shimazu, Y., Shimoji, K., Sumida, Y., Suzuki, M., Taniguchi, H., Tsuchiyama, H., Uesawa, D., Yokota, H., Yoshida, R., 2017. An Introduction to Himawari-8/9— Japan's New-Generation Geostationary Meteorological Satellites. *Meteorological Society of Japan*, Volume 94(2), pp. 151-183, https://doi.org/10.2151/jmsj.2016-009

Dozier, J., 1981. A method for satellite identification of surface temperature fields in subpixel resolution. *Remote Sens.*, 11, pp. 221-229, https://doi.org/0.1016/0034-4257(81)90021-3

Meteorological Satellite Center, "Himawari No. 8" and "Himawari No. 9", https://www.data.jma.go.jp/mscweb/ja/general/himawari.html (accessed on 9/13/2023)

Meteorological Satellite Center, Sample program, https://www.data.jma.go.jp/mscweb/ja/info/sample_data_program.html (accessed on 09/13/2023)

Mizutani, M., Takeuchi, W., Moriyama M., 2017. Wildfire detection in the Buryat Republic by Advanced Himawari-8 Imager (AHI), *Journal of the Japan society of Photogrammetry and Remote Sensing*, 56(5), pp. 244-247. (In Japanese), https://www.jstage.jst.go.jp/article/jsprs/56/5/56_244/_pdf

NASA, MODIS Thermal Anomalies and Fires, https://modis.gsfc.nasa.gov/data/dataprod/mod14.php (accessed on 9/13/2023)

Schmidt, C., 2012. GOES-R Advanced Baseline Imager (ABI) Algorithm Theoretical Basis Document For Fire / Hot Spot Characterization, Version 2.5. https://www.star.nesdis.noaa.gov/goesr/docs/ATBD/Fire.pdf

WWF Japan, Smoke Haze in Indonesia, Peat Fires Occurring in the Dry Season, https://www.wwf.or.jp/activities/basicinfo/3801.html (accessed on 09/13/2023)

Xu, W., Wooster, M. J., Kaneko, T., He, J., Zhang, T., & Fisher, D. 2017. Major advances in geostationary fire radiative power (FRP) retrieval over Asia and Australia stemming from use of Himarawi-8 AHI. *Remote Sens. of Environment*, 193, pp. 138-149. https://doi.org/10.1016/j.rse.2017.02.024